

Article

Considerations for the Design and Implementation of Ambient RF Signal Rectifiers in the 2.45 GHz WiFi Band

Joan J. Garcia-Garcia 

Grupo de Aplicaciones Electro-Magnéticas Industriales (GAEMI), Departament d'Enginyeria Electrònica, Universitat Autònoma de Barcelona (UAB), Cerdanyola del Vallès, 08193 Barcelona, Spain; joan.garcia@uab.cat

Abstract: Ambient RF energy harvesting (RF-EH) is a particular case of wireless power transfer (WPT), which is characterized by ultra-low power operation. This work points out theoretical and practical aspects that should be considered in the design of RF rectifiers for ambient RF energy harvesting systems. The most common RF rectifier circuits are compared and discussed using simulations and experimental data. The efficiency is analyzed in terms of the input power and load resistance. It is demonstrated that the most efficient RF rectifier in ultra-low power conditions is the simple diode capacitor structure. As an illustrative example, an RF rectifier has been fabricated by designing an impedance-matching network to operate into the WIFI band. The fabricated prototype shows a measured 12% efficiency working at 2.47 GHz with around -30 dBm ambient input power, which is higher than the reported efficiencies in the literature. The fabricated energy harvesting system delivers power between 25.6 nW and 129.6 nW to a resistive 10 k Ω load. The obtained results are applicable to ambient RF up to 6 GHz.

Keywords: RF-DC conversion efficiency; RF ambient energy harvesting; RF energy scavenging; ultra-low RF power rectifier



Citation: Garcia-Garcia, J.J. Considerations for the Design and Implementation of Ambient RF Signal Rectifiers in the 2.45 GHz WiFi Band. *Appl. Sci.* **2022**, *12*, 7884. <https://doi.org/10.3390/app12157884>

Academic Editor: Mengying Xie

Received: 8 July 2022

Accepted: 4 August 2022

Published: 5 August 2022

Publisher's Note: MDPI stays neutral with regard to jurisdictional claims in published maps and institutional affiliations.



Copyright: © 2022 by the author. Licensee MDPI, Basel, Switzerland. This article is an open access article distributed under the terms and conditions of the Creative Commons Attribution (CC BY) license (<https://creativecommons.org/licenses/by/4.0/>).

1. Introduction

Wireless Power Transfers (WPTs) have been a recurrent topic in the last decades generating numerous practical and commercial applications [1,2]. WPT typically ranges between 20 dBm and -30 dBm. Ambient RF-EH is situated in the ultra-low power extreme of this range, operating around and even below -30 dBm [3–7]. The possibility of feeding low-power devices by scavenging ambient RF energy is attractive for powering autonomous sensors [8] and IoTs general applications [9], especially in urban environments. More specifically, ambient RF harvesting has been recently evaluated for feeding Low Power Wide Area Networks (LPWANs) [3,10], wireless underground sensor networks (UWC) [11], or batteryless sensors [12]. As a consequence of the low power level, ambient RF-EH systems tend to operate in broadband or multiband configurations to enhance the system's performance [12–15]. The impedance matching between the antenna and the rectifier constitutes an important challenge in the case of multiband or broadband applications; however, there are promising approaches based on metamaterials [15]. The efficiency of an RF-EH system (η_{RF}) can be expressed as the product of the RF-EH constituent functional block efficiencies, as shown in Equation (1):

$$\eta_{RF} = \eta_{ant} \cdot \eta_{rec} \cdot \eta_{EMS} \cdot \eta_{sto} \quad (1)$$

where η_{ant} denotes antenna efficiency, η_{rec} denotes rectifier efficiency, η_{EMS} denotes energy management system efficiency, and η_{sto} denotes efficiency of the storage element. H_{rec} is defined as the ratio between the effective input power delivered to the rectifier by the antenna (P_{in}) and the power (P_{R_L}) delivered to the load resistor (R_L), as shown in Equation (2).

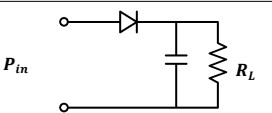
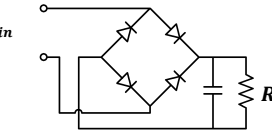
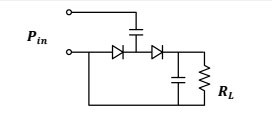
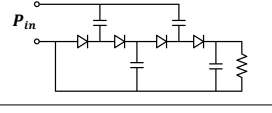
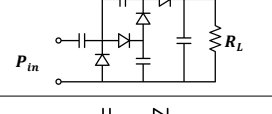
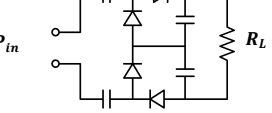
$$\eta_{rec} = \frac{P_{R_L}}{P_{in}} \quad (2)$$

If the antenna and the rectifier are not matched, a portion of the power delivered by the antenna to the rectifier is reflected in such a way that the effective power delivered to the rectifier (P_{in}) is a fraction of the nominal power delivered by the antenna at the rectifier input port (P_{nom}). The relation between P_{nom} and P_{in} and the reflection S-parameter (S_{11}) is provided by Equation (3).

$$P_{in} = P_{nom}(1 - |S_{11}|^2) \quad (3)$$

In a perfect match condition, $P_{in} = P_{nom}$ and the efficiency defined in Equation (2) is an intrinsic rectifier property independent from the impedances. Many RF rectifier circuits can be found in the literature operating in a wide range of frequencies, loads, and input power conditions. In [16–18], authors utilize a simple diode with an output capacitor in parallel with the load resistance. A four diode-bridge rectifier is used in [15,19–21]. In other cases, N-stage scalable Dickson or Greinacher architectures are used. These circuits combine rectification and output voltages that are proportional to the stage number (N). Dickson and Greinacher architectures are identical for $N = 1$ and are used in [22–24]. Second or higher-order Dickson rectifiers can be found in [23–25] and Greinacher structures in [26–28]. A first order Dickson–Greinacher full-wave variation can be found in [27,29–31]. Table 1 summarizes the efficiencies, input power, and load resistance in some of these examples operating at 2.45 GHz. In all cases, the rectifier and antenna impedance have been matched in such a way that the efficiencies of the different rectifiers are comparable. Despite the efficiency variations shown in Table 1, in most cases, the choice of the rectifier is barely justified.

Table 1. Examples of common RF-Rectifier Circuits operating @ 2.45 GHz.

	Ref.	P_{in}	R_L	Eff.	
Simple diode-capacitor rectifier	[16]	1 $\mu\text{W cm}^{-2}$	5.1 k Ω	45%	
	[17]	−6.6 dBm	6 k Ω	48%	
	[18]	−15 dBm	1.7 k Ω	28%	
Four-diode Bridge	[15]	−30 dBm	32 k Ω	8.8%	
	[19]	−9.2 dBm	10 k Ω	68%	
	[20]	−7.6 dBm	500 Ω	58%	
	[21]	17 dBm	350 Ω	50%	
Dickson-Greinacher N = 1	[22]	−20 dBm	2 k Ω	5%	
	[23]	−15 dBm	50 Ω	20%	
	[24]	−20 dBm	1 k Ω	17%	
Dickson N ≥ 2	[23]	−5 dBm	50 k Ω	70%	
	[25]	5 dBm	5 k Ω	59%	
	[24]	−20 dBm	1 k Ω	5%	
Greinacher N ≥ 2	[26]	13 dBm	20 k Ω	37.5%	
	[27]	−5 dBm	5 k Ω	10%	
	[28]	−7.5 dBm	300 Ω	9%	
Full-Wave Dickson Variation	[29]	9 dBm	6.7 k Ω	68%	
	[27]	−20 dBm	1.2 k Ω	6%	
	[30]	−27.5 dBm	14.7 k Ω	5%	
	[31]	−20 dBm	9 k Ω	12%	

The rectification is a passive highly nonlinear process that disperses the power of the input signal over the harmonic spectrum of the input signal's frequencies. Section 2 of this study is dedicated to theoretically analyzing the effects of this power dispersion in the rectifier's efficiency. In Section 3, harmonic balance simulations are used to compare the effect of P_{in} and R_L in the efficiency of the rectifiers included in Table 1. At the end of Section 3, simulated results are corroborated with experimental measurements of the

three rectifiers with higher efficiencies in ultra-low power conditions. Section 4 shows the fabrication and characterization of an ultra-low power RF rectifier operating in the WIFI band, pointing out some issues to consider in the implementation process. This work points out some practical and theoretical issues that should be considered when designing an ultra-low power RF rectifier for ambient RF harvesting systems.

2. Theoretical Limitations of the Rectifier's Efficiency

The rectification process is a nonlinear process with some characteristics that limit the efficiency, especially when operating at high frequency. The input power wave signal of the RF rectifier can be described using linear combinations of the wave complex variable \bar{a}_{in} defined in Equation (4):

$$\bar{a}_{in} = \frac{1}{2} \left(\frac{\bar{V}_{in}}{\sqrt{Z_{rec}}} + \sqrt{Z_{rec}} \bar{I}_{in} \right) \quad (4)$$

where \bar{V}_{in} and \bar{I}_{in} are the voltage and current complex variables at the rectifier input port, and Z_{rec} is the rectifier input impedance (in general a complex number). The rectifier input-power complex variable can be obtained from the \bar{a}_{in} variable following Equation (5).

$$\bar{P}_{in} = \frac{1}{2} \bar{a}_{in} \bar{a}_{in}^* \quad (5)$$

The input power (P_{in}) is obtained by averaging the corresponding temporal expression of \bar{P}_{in} over a period. It can be shown that only the DC, ω_0 , and the harmonics contribute to the P_{in} averaged value. The power dispersion over the harmonic spectrum in the rectification process is described by the Fourier series of the rectifier wave. Equations (6) and (7) show the Fourier series of a half- (f_{hrw}) and full-rectified (f_{frw}) waves of a sinusoidal signal with amplitude A and angular frequency ω_0 .

$$f_{hrw} = \frac{A}{\pi} + \frac{A}{2} \sin(\omega_0 t) - \frac{2A}{\pi} \sum_{n=1}^{\infty} \frac{\cos(2n\omega_0 t)}{4n^2 - 1} \quad (6)$$

$$f_{frw} = \frac{2A}{\pi} - \frac{4A}{\pi} \sum_{n=1}^{\infty} \frac{\cos(2n\omega_0 t)}{4n^2 - 1} \quad (7)$$

The DC power component directly delivers a fraction of the input power to the load. The rest of the input power is spitted in the harmonic signal spectrum. Impedance matching networks are designed to guarantee that the input wave at the operating frequency is not reflected. However, RF systems are not matched for all frequencies, and harmonic components different from the matched wave will be mainly reflected when $S_{11} \leq -3$ dB. The numerical evaluation of the DC and the fundamental frequency points out a 67% limit for the half-wave rectifier and a 64% for the full-wave rectifier in a matched system operating at the fundamental frequency (see Table 2).

Therefore, in the case of a perfect impedance matching at the input signal frequency, a similar performance is expected for the half-wave and full-wave rectifier (67% and 64%, respectively). Depending on the return losses at the second harmonic, these efficiencies can be increased up to 82% in the case of the half-wave rectifier and up to 94% in the case of the full-wave rectifier.

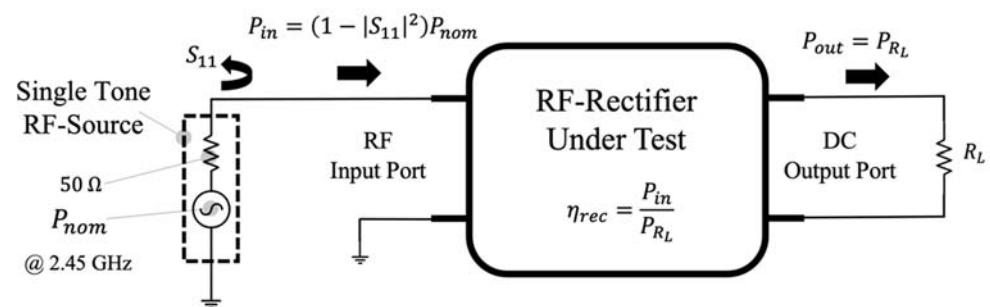
This maximum efficiency values are degraded by the losses in the lumped elements at low input power and by the diode breakdown voltage V_{Br} at high input power [4], as observed in Figures 2–4 in the following section. In the case of high input power, the maximum DC power across the diode is limited by the reverse breakdown voltage in such a manner that $V_{DC \text{ diode max}} = \frac{V_{Br}}{2}$. Consequently, the maximum DC power that a rectifier can deliver to the load is given by $P_{DC \text{ MAX}} = \frac{V_{Br}^2}{4R_L}$. This limitation of the output power produces a quick efficiency drop, as P_{in} grows beyond some specific value that may vary depending on the rectifier's architecture [32].

Table 2. Harmonic coefficients of the full- and half-rectifier waves and the associate power.

Frequency Component	Half-Wave Rectifier (f_{hrw})			Full-Wave Rectifier (f_{frw})		
	Fourier Coefficient	Output Power Coefficient	Input Power Percentage	Fourier Coefficient	Output Power Coefficient	Input Power Percentage
DC	$\frac{A}{\pi}$	$\frac{1}{\pi} = 0.32$	67%	$\frac{2A}{\pi}$	$\frac{2}{\pi} = 0.64$	64%
f_o	$\frac{A}{2}$	$\frac{1}{\sqrt{2}\pi} = 0.35$		–	–	
$2f_o$	$\frac{2A}{3\pi}$	$\frac{2}{3\sqrt{2}\pi} = 0.15$	15%	$\frac{4A}{3\pi}$	$\frac{4}{3\sqrt{2}\pi} = 0.30$	30%
$3f_o$	–	–	–	–	–	–
$4f_o$	$\frac{2A}{15\pi}$	$\frac{2}{15\sqrt{2}\pi} = 0.03$	3%	$\frac{4A}{15\pi}$	$\frac{4}{15\sqrt{2}\pi} = 0.0$	6%
\vdots	\vdots	\vdots	\vdots	\vdots	\vdots	\vdots

3. Parametric Analysis of RF Rectifier Circuits Efficiency

As it has been commented, the choice of an architecture for the RF rectification is barely justified in many examples that can be found in the literature. In the case of the design of a rectifier for ambient RF that is destined to operate in ultra-low power conditions, the most important parameter is the efficiency. To determine the best rectifier for this specific conditions, Table 1 rectifiers have been simulated using ADS-harmonic balance analyses to evaluate and compare the efficiencies. Each rectifier circuit has a particular input impedance that reflects a fraction of the injected power (P_{nom}). The intrinsic efficiency defined in Equation (2) is referred to the effective power delivered to the load (P_{in}). Therefore, it is a magnitude independent from the input impedance that can be compared between different rectifiers. Figure 1 shows the harmonic-balance simulation setup used to evaluate the intrinsic rectifier efficiency of different rectifiers.

**Figure 1.** Simulation setup to evaluate the intrinsic efficiency η_{rec} of the different rectifiers included in Table 1, using harmonic balance analysis with a 50 Ω single-tone source operating at 2.45 GHz.

The different rectifier circuits have been simulated using identical elements. The SMS-7630 Schottky diode model has been chosen because of its low forward voltage (ranging from 60 to 120 mV at 0.1 mA [33]). The rectifier output capacitors have been fixed to the standard value of 4.7 μF in all cases for the simulations. The analysis of the efficiency as a bidimensional function on P_{in} and R_L points out the existence of different combinations that optimize the efficiency. Figure 2 shows, as example, the simulated $\eta_{rec}(P_{in}, R_L)$ for the N = 2 Dickson rectifier circuit. As it can be observed, there are multiple P_{in} and R_L combinations producing the maximum efficiency (close to 70%). It is also observed that for the expected ambient RF power ($P_{in} \leq -30$ dBm), the maximum DC conversion efficiencies are lower than 30%, which are higher than 10% only in the range of $1 \text{ k}\Omega < R_L < 300 \text{ k}\Omega$. The efficiency mapping in Figure 2 offers a good overview of the efficiency general behavior but renders the comparison between rectifiers difficult.

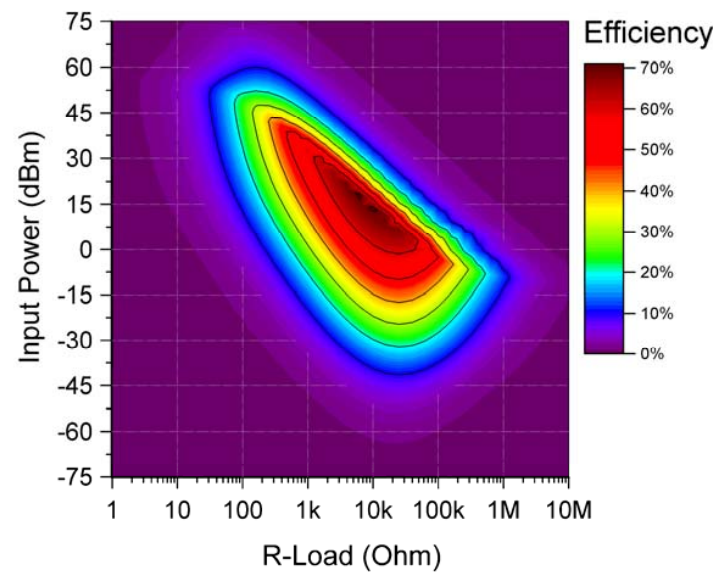


Figure 2. Representation of the simulated intrinsic efficiency function $\eta_{rec}(P_{in}, R_L)$ for $N = 2$ Dickson RF rectifier operating at 2.45 GHz.

Figure 3a shows intrinsic efficiencies as a function of the nominal power (P_{nom}) for $R_L = 10 \text{ k}\Omega$, and a curve for each different rectifier can be observed. However, since the input impedance of each rectifier is different, the curves in Figure 3a are not comparable. Figure 3b shows the same data plotted as a function of P_{in} enabling the comparison. It can be observed that, in Figure 3b, only four different traces are appreciated, because $N = 2$ Dickson, $N = 2$ Greinacher, and the full wave variation rectifier efficiencies are degenerated in this representation. It can be observed that the more complex circuits ($N = 2$ and full wave variation) offer better efficiencies at higher input power ($P_{in} > 0 \text{ dBm}$). However, for low and ultra-low input power ($P_{in} \leq -30 \text{ dBm}$), the best efficiencies correspond to the simple diode-capacitor rectifier, $N = 1$ Dickson-Greinacher rectifier, and four-bridge rectifier.

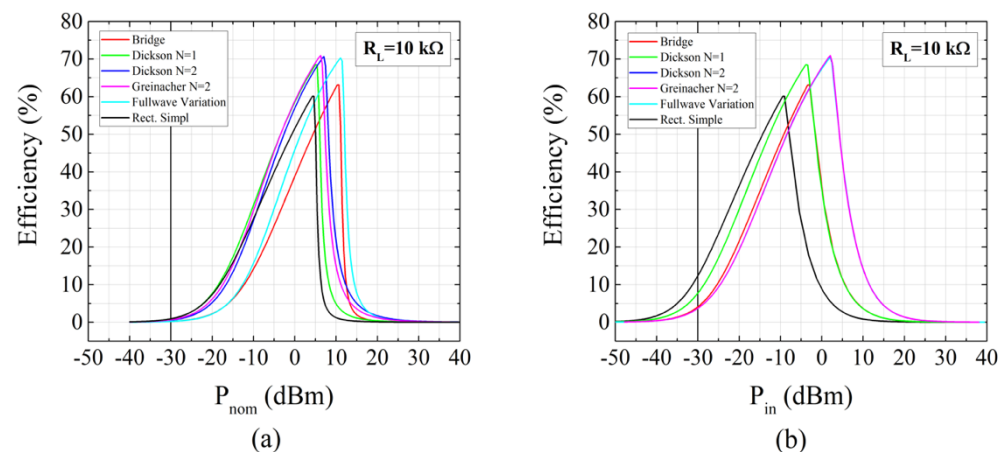


Figure 3. Simulated rectifier efficiency for the six circuits in Table 1 as a function of P_{nom} in (a) and as a function of P_{in} in (b).

In ultra-low power operation conditions ($P_{in} \leq -30 \text{ dBm}$), it can be observed that the best efficiency is around 12% and corresponds to the simple diode-capacitor rectifier. The second-best performance is obtained with the first order $N = 1$ Dickson–Greinacher rectifier (around 8%) and finally the four-diode rectifier with less than 4% efficiency.

Figure 4 shows the intrinsic efficiency $\eta_{rec}(P_{in}, R_L)$ for $R_L = 100 \Omega$ (Figure 4a) and for $R_L = 100 \text{ k}\Omega$ (Figure 4b). In both cases, the load is far from the optimum values

(around 10 k Ω), and maximum efficiencies are lower than 50%. In the case of low load impedances ($R_L \sim 100 \Omega$), the best efficiencies correspond to the four-diode bridge rectifier for $P_{in} \geq 0$ dBm. However, under high load-resistance conditions ($R_L \sim 100 \text{ k}\Omega$), the best performance corresponds to both the second-order Dickson and Greinacher rectifiers and are achieved in the range of $-20 \text{ dBm} \leq P_{in} \leq 15 \text{ dBm}$. In both cases, the conversion efficiency under ultra-low power ($P_{in} \leq -30 \text{ dBm}$) is lower than 2% for $R_L = 100 \Omega$ and 5% for $R_L = 100 \text{ k}\Omega$. Even in the extreme loads described in Figure 4, the simple diode-capacitor rectifier (Rect. Simple) efficiency is not below the other rectifiers.

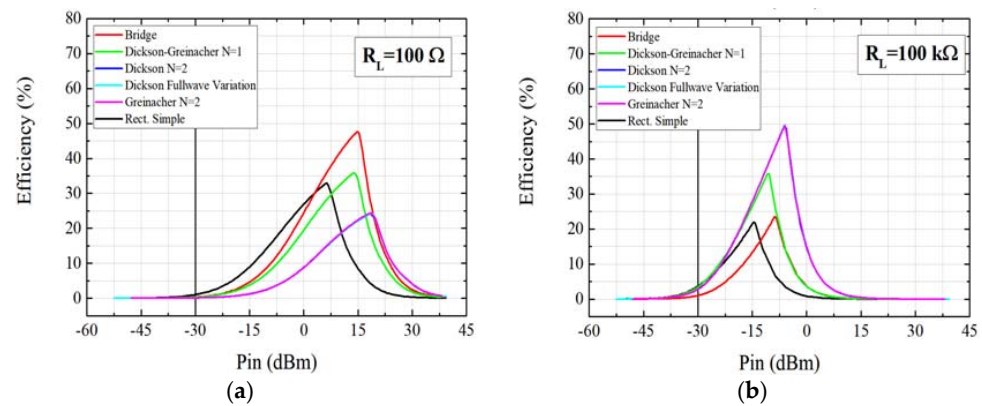


Figure 4. Simulated $\eta_{rec}(P_{in}, R_L)$ for $R_L = 100 \Omega$ (a) and $R_L = 100 \text{ k}\Omega$ (b).

Results in Figures 3 and 4 discard the utilization of Dickson and Greinacher high-order rectifiers at ultra-low power. Figure 5 shows the simulated efficiency as a function of the load resistance for the three best rectifiers identified in Figures 4 and 5. As observed, the maximum efficiency of 12.8% corresponds to the simple diode-capacitor rectifier loaded with $R_L = 4.5 \text{ k}\Omega$. The second-best efficiency corresponds to the first-order Dickson–Greinacher rectifier, which is considerably lower, showing an efficiency of 7.8% when loaded with $R_L = 8.9 \text{ k}\Omega$. The four-diode bridge rectifier is the less efficient rectifier showing a maximum of 4.3% for $R_L = 5 \text{ k}\Omega$. The better performance of the diode-capacitor rectifier at ultra-low input power is attributable to its simpler structure that minimizes losses due to parasitic impedances in the constituent elements.

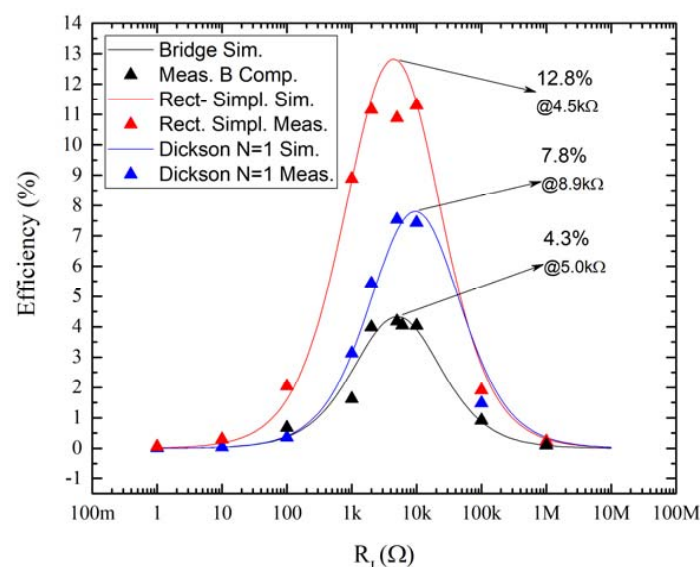


Figure 5. ADS-harmonic balance simulated (blue, red, and black lines) and measured (blue, red, and black dots) efficiencies for simple diode-capacitor rectifier, four-diode Bridge rectifier, and the first-order Dickson–Greinacher rectifier circuits. $P_{in} = -30 \text{ dBm}$. The optimal efficiencies and R_L values for each rectifier are labelled.

Simulated results in Figure 5 have been corroborated with experimental measurements using an experimental setup that reproduces the simulation setup Figure 1. A vector analyzer with zero span has been used as a $50\ \Omega$ input source at 2.45 GHz, with $P_{nom} = -30$ dBm. The same vector analyzer measures the S_{11} parameter needed to evaluate the power delivered to the rectifier (P_{in}) according to Equation (3). The rectifiers under test have been fabricated by minimizing connection paths using a FR4 PCB prototype board. The output DC voltage has been measured with a N6781A SMU in a four-wire voltage measurement configuration by averaging the output voltage. R_L values have been generated with a standard resistor decade box.

Experimental measurements show a good agreement with the simulated results. The above analysis shows that the diode capacitor circuit is the most efficient rectifier operating at -30 dBm, achieving efficiencies higher than 10% for loads between $1\ \text{k}\Omega$ and $10\ \text{k}\Omega$.

4. Ambient RF Energy Harvesting Prototype Performance in Real Conditions

Numerical and experimental data discussed in the previous sections show that the most efficient RF rectifier for $P_{in} = -30$ dBm is the simple diode-capacitor circuit when $1\ \text{k}\Omega \leq R_L \leq 10\ \text{k}\Omega$. The implementation of an ambient RF energy harvester is conditioned by practical issues related with the impedance-matching network that should be considered. Theoretically, a lumped C-L impedance network can be used to match the diode-capacitor rectifier with the standard $50\ \Omega$ antenna. However, tolerances and parasitic capacitances and inductances of the lumped elements complicate the fabrication of the prototype. All these effects can be compensated by tuning the constituent elements of the impedance matching network.

Figure 6 shows the picture of the implemented prototype of an RF rectifier. The matching network has been initially designed by using the ADS Smith chart, taking into account the measured input impedance of the fabricated diode-capacitor rectifier. The final values of the impedance matching network have been tuned to optimize the adaptation. Figure 7 shows the measurements of a fabricated RF diode-capacitor rectifier prototype finally matched at 2.47 GHz for -30 dBm input power. The impedance-matching network is a C-L network with $C = 0.1\ \text{pF}$ and $L = 6\ \text{nH}$, as shown Figure 7a's inset. Figure 7b shows the measured input impedance of the matched rectifier (Z_{rec}) at the operating frequency.

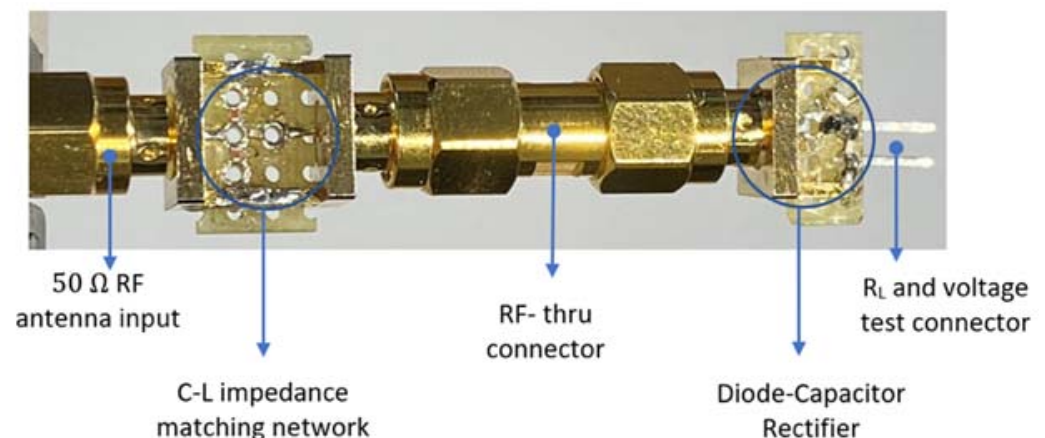


Figure 6. Implemented prototype of an ambient RF energy harvesting system composed by the input antenna port, the C-L impedance network, a thru connector, the diode-capacitor rectifier, and a connector to the load resistor. Fabrications have been performed using the following: SMS-7630 [33] diode, capacitors from the HiQ-CBR Series, Case Size 0402 Radio Frequency and Microwave Ceramic Capacitor Kit from Kemet, and the inductors from the High Frequency Inductor Designer Kit EIA 0402 from Johanson Technology.

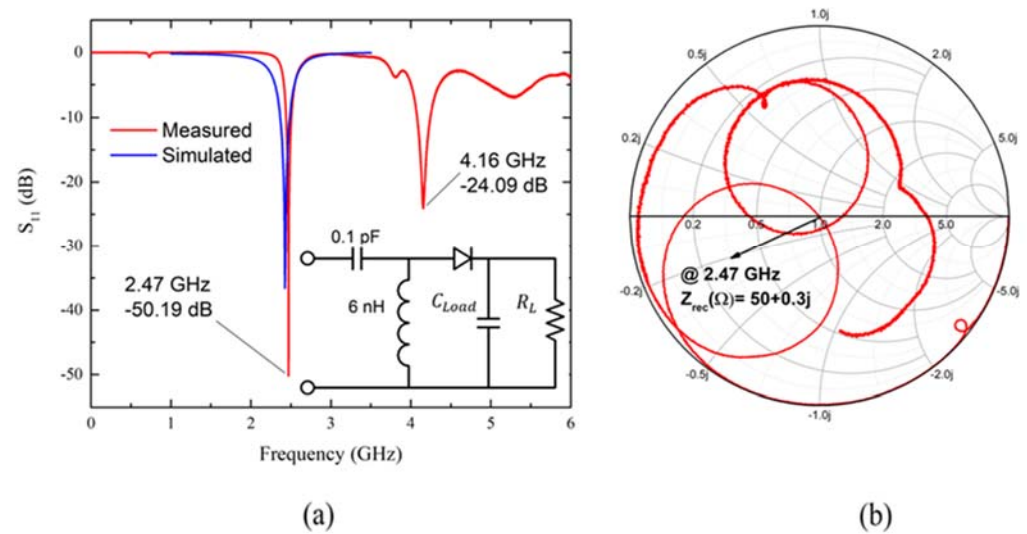


Figure 7. Measured and simulated S_{11} parameter (a) and impedance in the Smith Chart (b) of a fabricated RF-rectifier prototype matched at 2.45 GHz for -30 dBm input power. Fabrication has been done using: SMS-7630 [33], $C_{Load} = C_{RF} + C_{sto}$ being $C_{RF} = 2.2$ pF, $C_{sto} = 6.8$ mF; $R_L = 10$ k Ω and $C_m = 0.1$ pF using a CBR04C108B1GAC RF-capacitor and $L_m = 6$ nH L-07C12NJV6S RF-autoinduction for the matching circuit. Simulated S_{11} only have sense below the series resonant frequency of the RF inductor used (3.5 GHz).

Figure 8 overlaps the measured S_{11} parameter of the fabricated and matched RF rectifier prototype with the power max-hold measurement of the ambient RF spectrum in our laboratory. As observed, the matching frequency coincides with one of the active channels of the WIFI band. The efficiencies shown in Figure 5 indicate that only 10% of -30 dBm (1 μ W) input power would be delivered to a 10 k Ω load, producing a maximum of 32 mV voltage and supplying 33.2 μ A to the load. However, it must be considered that the ambient RF signals are constantly oscillating depending on the wireless traffic. As a result of these fluctuations, the real effective output power delivered to the load will be lower than that indicated by Figure 5 efficiencies.

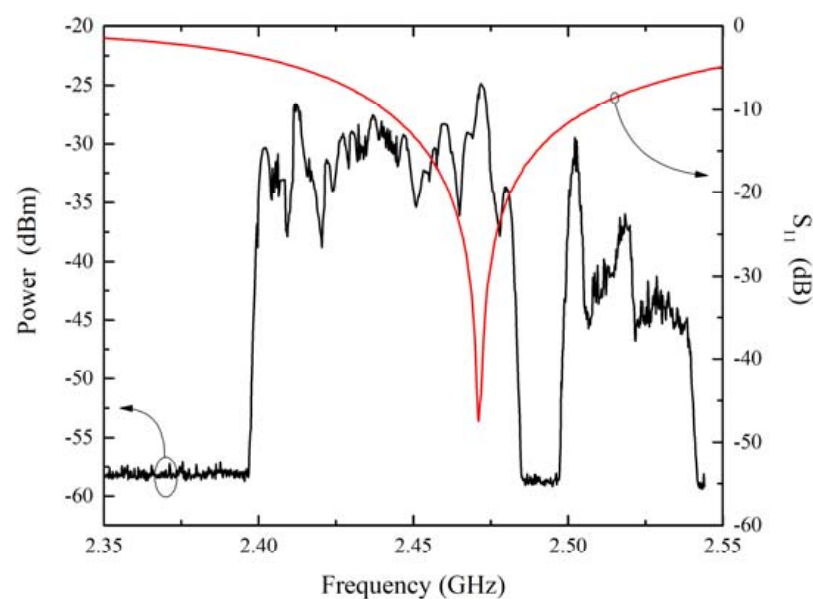


Figure 8. Max-hold ambient RF power spectrum measurement, between 2.35 GHz and 2.55 GHz (in black and left-scale); S_{11} of the RF rectifier with 6.8 mF and 10 k Ω load in the output (in red and right scale).

As observed in Figure 9, the output voltage oscillates between 16 mV and 36 mV corresponding to 25.6 nW and 129.6 nW. In the low voltage region, the harvesting system can supply 2.5 μ A, which should be enough to power ultra-low commercial power sensors. However, for a proper power function, several systems should be combined to achieve the minimum voltage requirements.

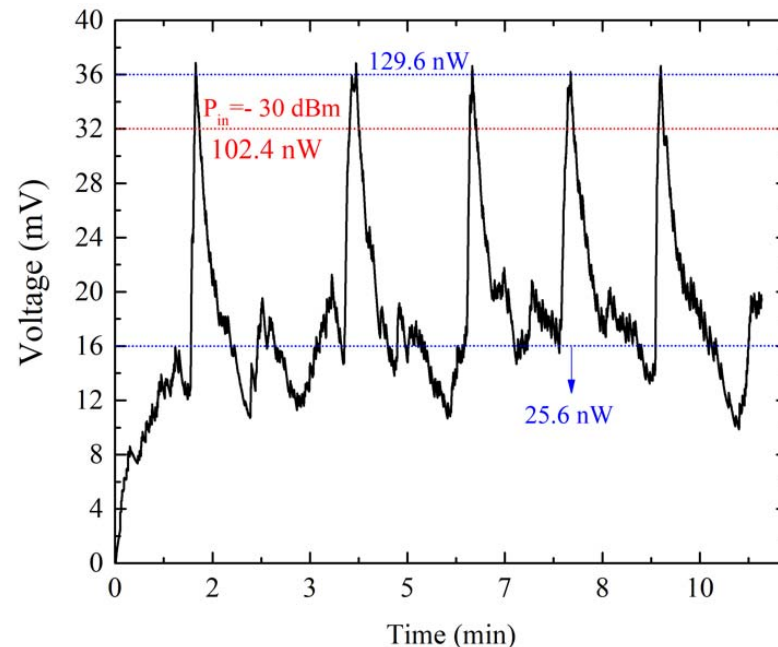


Figure 9. Measured output voltage in the 10 k Ω output resistance produced by the ambient RF energy harvesting. The red line indicates the voltage and power level corresponding to a -30 dBm input power. The blue lines indicate the maximum and minimum voltage and power supplied by the RF harvesting system.

5. Conclusions

The efficiency of the most common RF rectifier circuits has been compared side-by-side using simulations and experimental data. It has been shown that the simple diode-capacitor RF rectifier is the most efficient choice when operating in ultra-low input-power conditions. The fabricated prototype has shown to be suitable for powering ultra-low power sensors in the standby stage using the ambient RF energy. There are two clear methods for improving the RF energy harvested by the described prototype: first, designing a broadband matching network that takes advantage of the energy in all the communication band, and the second possibility is to combine several rectifiers in a power network to increase the output voltage and the final stored charge.

Funding: This research has been founded by the Grupo de Aplicaciones Electro-Magnéticas Industriales (GAEMI) of the Departament d'Enginyeria Electrònica of the Universitat Autònoma de Barcelona.

Institutional Review Board Statement: Not applicable.

Informed Consent Statement: Not applicable.

Data Availability Statement: Not applicable.

Conflicts of Interest: The author declares no conflict of interest.

References

1. Cansiz, M.; Altinel, D.; Kurt, G.K. Efficiency in RF energy harvesting systems: A comprehensive review. *Energy* **2019**, *174*, 292–309. [CrossRef]
2. PowerCast. P2110-915 MHz RF Powerharvester Receiver Data Sheet. 2018. Available online: <https://www.powercastco.com/> (accessed on 1 July 2022).
3. Finnegan, J.; Niotaki, K.; Brown, S. Exploring the boundaries of ambient rf energy harvesting with lorawan. *IEEE Internet Things J.* **2021**, *8*, 5736–5743. [CrossRef]
4. Wagih, M.; Weddell, A.S.; Beeby, S. Millimeter-Wave Power Harvesting: A Review. *IEEE Open J. Antennas Propag.* **2020**, *1*, 560–578. [CrossRef]
5. Luo, Y.; Pu, L.; Wang, G.; Zhao, Y. RF energy harvesting wireless communications: Rf environment, device hardware and practical issues. *Sensors* **2019**, *19*, 3010. [CrossRef] [PubMed]
6. Jayakody, D.N.K.; Thompson, J.; Chatzinotas, S.; Durrani, S. *Wireless Information and Power Transfer: A New Paradigm for Green Communications*; Springer International Publishing: Cham, Switzerland, 2017.
7. Gu, X.; Grauwin, L.; Dousset, D.; Hemour, S.; Wu, K. Dynamic Ambient RF Energy Density Measurements of Montreal for Battery-Free IoT Sensor Network Planning. *IEEE Internet Things J.* **2021**, *8*, 13209–13221. [CrossRef]
8. Kim, S.; Vyas, R.; Bito, J.; Niotaki, K.; Collado, A.; Georgiadis, A.; Tentzeris, M.M. Ambient RF energy-harvesting technologies for self-sustainable standalone wireless sensor platforms. *Proc. IEEE* **2014**, *102*, 1649–1666. [CrossRef]
9. Luo, Y.; Pu, L. Practical Issues of Energy Harvesting and Data Transmissions in Sustainable IoT. *arXiv* **2019**. [CrossRef]
10. Peruzzi, G.; Pozzebon, A. A review of energy harvesting techniques for low power wide area networks (LPWANs). *Energies* **2020**, *13*, 3433. [CrossRef]
11. Raza, U.; Salam, A. On-site and external energy harvesting in underground wireless. *Electronics* **2020**, *9*, 681. [CrossRef]
12. Muncuk, U.; Alemдар, K.; Sarode, J.D.; Chowdhury, K.R. Multiband ambient RF energy harvesting circuit design for enabling batteryless sensors and IoT. *IEEE Internet Things J.* **2018**, *5*, 2700–2714. [CrossRef]
13. Pinuela, M.; Mitcheson, P.D.; Lucyszyn, S. Ambient RF energy harvesting in urban and semi-urban environments. *IEEE Trans. Microw. Theory Tech.* **2013**, *61*, 2715–2726. [CrossRef]
14. Yang, L.; Zhou, Y.J.; Zhang, C.; Yang, X.M.; Yang, X.-X.; Tan, C. Compact Multiband Wireless Energy Harvesting Based Battery-Free Body Area Networks Sensor for Mobile Healthcare. *IEEE J. Electromagn. RF Microwaves Med. Biol.* **2018**, *2*, 109–115. [CrossRef]
15. Coskuner, E.; Garcia-Garcia, J. Metamaterial impedance matching network for ambient rf-energy harvesting operating at 2.4 GHz and 5 GHz. *Electronics* **2021**, *10*, 1196. [CrossRef]
16. Vandelle, E.; Bui, D.H.N.; Vuong, T.-P.; Ardila, G.; Wu, K.; Hemour, S. Harvesting Ambient RF Energy Efficiently with Optimal Angular Coverage. *IEEE Trans. Antennas Propag.* **2019**, *67*, 1862–1873. [CrossRef]
17. Hu, Y.-Y.; Sun, S.; Xu, H.; Sun, H. Grid-Array Rectenna with Wide Angle Coverage for Effectively Harvesting RF Energy of Low Power Density. *IEEE Trans. Microw. Theory Tech.* **2019**, *67*, 402–413. [CrossRef]
18. Palazzi, V.; Kalialakis, C.; Alimenti, F.; Mezzanotte, P.; Roselli, L.; Collado, A.; Georgiadis, A. Design of a ultra-compact low-power rectenna in paper substrate for energy harvesting in the Wi-Fi band. In Proceedings of the 2016 IEEE Wireless Power Transfer Conference (WPTC), Aveiro, Portugal, 5–6 May 2016; pp. 23–26. [CrossRef]
19. Karampatea, A.; Siakavara, K. Synthesis of rectenna for powering micro-watt sensors by harvesting ambient RF signals' power. *Electronics* **2019**, *8*, 1108. [CrossRef]
20. Karampatea, A.; Siakavara, K. Hybrid rectennas of printed dipole type on Double Negative Dielectric Media for powering sensors via RF ambient energy harvesting. *AEU-Int. J. Electron. Commun.* **2019**, *108*, 242–250. [CrossRef]
21. Chang, Y.; Zhang, P.; Wang, L. Highly efficient differential rectenna for RF energy harvesting. *Microw. Opt. Technol. Lett.* **2019**, *61*, 2662–2668. [CrossRef]
22. Song, C.; Huang, Y.; Carter, P.; Zhou, J.; Joseph, S.D.; Li, G. Novel Compact and Broadband Frequency-Selectable Rectennas for a Wide Input-Power and Load Impedance Range. *IEEE Trans. Antennas Propag.* **2018**, *66*, 3306–3316. [CrossRef]
23. Li, P.; Long, Z.; Yang, Z. RF Energy Harvesting for Batteryless and Maintenance-Free Condition Monitoring of Railway Tracks. *IEEE Internet Things J.* **2021**, *8*, 3512–3523. [CrossRef]
24. Marshall, B.R.; Morys, M.M.; Durgin, G.D. Parametric analysis and design guidelines of RF-to-DC Dickson charge pumps for RFID energy harvesting. In Proceedings of the 2015 IEEE International Conference on RFID (RFID), San Diego, CA, USA, 15–17 April 2015; pp. 32–39. [CrossRef]
25. Cheng, L.W.; Gnanagurunathan, G. Two-Stage Dickson Charge Pump Rectifier with Harmonics Suppression for 2.45 GHz WPT. In Proceedings of the 2020 IEEE International RF and Microwave Conference (RFM), Kuala Lumpur, Malaysia, 14–16 December 2020; pp. 15–18. [CrossRef]
26. Fan, S.; Yuan, Z.; Gou, W.; Member, S.; Zhao, Y. A 2.45-GHz Rectifier-Booster Regulator With Impedance Matching Converters for Wireless Energy Harvesting Shiquan. *IEEE Trans. Microw. Theory Tech.* **2019**, *67*, 3833–3843. [CrossRef]
27. Berges, R.; Fadel, L.; Oyhenart, L.; Vigneras, V.; Taris, T. Conformable dual-band wireless energy harvester dedicated to the urban environment. *Microw. Opt. Technol. Lett.* **2020**, *62*, 3391–3400. [CrossRef]
28. Curty, J.-P.; Joehl, N.; Krummenacher, F.; Dehollain, C.; Declercq, M.J. A model for μ -power rectifier analysis and design. *IEEE Trans. Circuits Syst. I Regul. Pap.* **2005**, *52*, 2771–2779. [CrossRef]

29. Chandravanshi, S.; Akhtar, M.J. An efficient dual-band rectenna using symmetrical rectifying circuit and slotted monopole antenna array. *Int. J. RF Microw. Comput. Eng.* **2020**, *30*, e22117. [[CrossRef](#)]
30. Song, C.; Huang, Y.; Zhou, J.; Zhang, J.; Yuan, S.; Carter, P. A high-efficiency broadband rectenna for ambient wireless energy harvesting. *IEEE Trans. Antennas Propag.* **2015**, *63*, 3486–3495. [[CrossRef](#)]
31. Zhang, H.; Zhong, Z.; Guo, Y.-X.; Wu, W. Differentially-fed charge pumping rectifier design with an enhanced efficiency for ambient RF energy harvesting. In Proceedings of the 2017 IEEE MTT-S International Microwave Symposium (IMS), Honolulu, HI, USA, 4–9 June 2017; pp. 613–616. [[CrossRef](#)]
32. Valenta, C.R.; Durgin, G.D. Harvesting wireless power: Survey of energy-harvester conversion efficiency in far-field, wireless power transfer systems. *IEEE Microw. Mag.* **2014**, *15*, 108–120. [[CrossRef](#)]
33. Skyworks Solutions. Surface Mount Mixer and Detector Schottky Diodes. Data Sheet. 2016. Available online: <https://www.skyworksinc.com/-/media/A36775836A4E4BA8A92104088692424F.ashx> (accessed on 1 March 2021).